

Optical Response of Periodic Arrays of Graphene Nanodisks

Juan R. Deop-Ruano¹, Stephen Sanders², Alessandro Alabastri², Wilton J. M. Kort-Kamp³, Diego A. R. Dalvit⁴, and Alejandro Manjavacas^{1,5,*}

¹*Instituto de Óptica (IO-CSIC), Consejo Superior de Investigaciones Científicas, Madrid 28006, Spain*

²*Department of Electrical and Computer Engineering, Rice University, Houston, Texas 77005, USA*

³*Theoretical Division, MS B262, Los Alamos National Laboratory, Los Alamos, New Mexico 87545, USA*

⁴*Theoretical Division, MS B213, Los Alamos National Laboratory, Los Alamos, New Mexico 87545, USA*

⁵*Department of Physics and Astronomy, University of New Mexico, Albuquerque, New Mexico 87106, USA*



(Received 18 July 2022; revised 13 September 2022; accepted 27 September 2022; published 28 October 2022)

Doped graphene nanostructures are a promising platform for photonics due to their exceptionally strong and tunable plasmonic resonances. When placed in a periodic array configuration, the plasmons supported by the individual nanostructures interact with each other and, under the appropriate conditions, can give rise to a collective mode known as a lattice resonance. Here, we perform a comprehensive analysis of the response of periodic arrays of graphene nanodisks and identify the conditions under which the system is able to support lattice resonances. We find that the ratio between the period of the array and the wavelength of the plasmon completely determines the behavior of the system. As a consequence, strong lattice resonances are achieved for micron-size nanodisks in the terahertz regime. We develop a theoretical model valid beyond the electrostatic approximation and use it to derive closed analytical expressions for the strength, the wavelength, and the width of the optical resonance of the arrays. The theoretical framework developed in this work paves the way for facile design and discovery of emerging properties of periodic arrays of graphene nanostructures that could enable applications in photonics and plasmonics.

DOI: 10.1103/PhysRevApplied.18.044071

I. INTRODUCTION

Nanostructures carved out from graphene monolayers are exceptional platforms for the manipulation of light at the nanoscale [1,2]. When doped with charge carriers (i.e., electrons or holes), these systems support localized plasmons that lead to very strong optical cross sections with record levels of field confinement [3]. Furthermore, the wavelength of these plasmons can be tuned by modifying the number of carriers in the nanostructure, which can be achieved, for example, through electrostatic gating [4–6]. Thanks to their exceptional optical properties, graphene nanostructures have been proposed as a platform for a variety of applications, principally in the terahertz regime [7]. These applications range from biosensing [8–14] to the enhancement of dipole-forbidden transitions [15–18], and nonlinear effects [19,20], as well as the implementation of polarizers, modulators, absorbers [21–24], and even time-varying metasurfaces [25].

In order to fully exploit the potential offered by graphene nanostructures, it is necessary to develop theoretical tools capable of efficiently describing their optical response. In

this context, the plasmon wave function (PWF) formalism has been shown to provide an accurate description of the localized plasmon resonances supported by individual graphene nanostructures of arbitrary shape, when their sizes are much smaller than the wavelength of the light used to excite them [3,26,27]. Nevertheless, many interesting applications rely on using ensembles of nanostructures ordered in a periodic arrangement. In such case, it is well known that the interaction between the localized plasmons supported by the nanostructures can give rise to collective responses that can be very different from those of the individual constituents [28]. A paradigmatic example are lattice resonances, which are collective modes that emerge from the coherent multiple scattering enabled by the periodicity of the array [29–31]. Because of their collective character, these resonances display very narrow lineshapes, which give rise to quality factors that are significantly larger than those of the localized plasmons. For that reason, lattice resonances are being exploited in applications such as nanoscale light emission and color generation [29–31], to cite a few.

However, despite the extensive research effort devoted to studying the plasmonic response of graphene nanostructures, the prospect of using them to support lattice resonances remains largely unexplored. Here, we

*a.manjavacas@csic.es

investigate the response of periodic arrays of graphene nanodisks and analyze its dependence on the different geometrical and material properties of the system. To that end, we first introduce electrodynamic corrections to the PWF formalism and then combine it with the coupled dipole model (CDM) [28,32–36]. The resulting approach allows us to derive analytical expressions for the spectral position, the strength, and the quality factor of the resonances supported by the array. We identify two different regimes determined by the relative value of the period of the array a and the resonance wavelength of the localized plasmon of the individual nanodisks λ_p . For $a < \lambda_p$, the response of the array resembles that of the localized plasmon supported by the nanodisks, resulting in a strong extinction but a relatively small quality factor. On the contrary, when $a > \lambda_p$, the array can support collective lattice resonances that produce a weaker extinction but with a much larger quality factor. The results of this work provide a simple yet accurate theoretical framework that facilitates the design and implementation of applications exploiting the exceptional properties of periodic arrays of graphene nanodisks.

II. RESULTS

We start by considering an individual graphene nanodisk of diameter D , doped to a Fermi energy E_F , which is placed in the xy plane and surrounded by vacuum. The response of this nanostructure can be described using the PWF formalism [3,13,16,18,26,27]. This approach is based on the electrostatic approximation and, therefore, assumes that the size of the nanodisk is much smaller than the wavelength of light λ , such that $kD \ll 1$ with $k = 2\pi/\lambda$. Using the PWF formalism, and considering only the lowest order dipolar mode, we can write the electrostatic polarizability of a nanodisk as [3,13,27]

$$\alpha_0 = \frac{D^3 \xi^2}{-1/\eta - i\omega D/\sigma}, \quad (1)$$

where $\eta = -0.07249$ and $\xi = 0.85020$ are constants [18, 26], $\omega = 2\pi c/\lambda$ is the angular frequency, and σ represents the electric conductivity of graphene, which we describe using the Drude model as $\sigma = (ie^2 E_F / \pi \hbar^2) / (\omega + i\gamma)$. In this expression, $\gamma = ev_F^2 / (\mu E_F)$ is the damping coefficient with $v_F \approx c/300$ being the Fermi velocity of graphene and μ the electron mobility. Here, we assume that $\mu = 10^4 \text{ cm}^2/\text{Vs}$, a value that is within experimental reach [37–39]. The electrostatic polarizability defined in Eq. (1) displays a dipolar plasmon resonance with wavelength

$$\lambda_{p,0} = \frac{2\pi c \hbar}{e} \sqrt{|\eta| \pi} \sqrt{\frac{D}{E_F}}. \quad (2)$$

In this work, we aim to explore arrays of graphene nanodisks with resonances in the terahertz regime, for which

the localized plasmon resonances of their constituents have a wavelength of the same order as the array period, i.e., $\lambda_p \sim a$. Therefore, we consider graphene nanodisks with sizes of $D = 10 \mu\text{m}$ and $D = 20 \mu\text{m}$ and doping levels in the range $E_F = 0.4\text{--}1.0 \text{ eV}$. As demonstrated by previous works [3,40–42], this range of Fermi energies is within experimental reach. Furthermore, using Eq. (2), these systems are expected to have localized plasmon resonances in the wavelength range from 50 to 110 μm (i.e., approximately 3 THz to approximately 6 THz). This means that the condition $kD \ll 1$ may not be fully satisfied and, therefore, in order to obtain an accurate description of the response of the nanodisks, we need to incorporate the appropriate electrodynamic corrections to α_0 . To do so, we need to calculate the electrodynamic depolarization field that the dipole induced in the nanodisk produces on itself. Following the derivation shown in Appendix A, the corrected polarizability is given by

$$\alpha = \left(\alpha_0^{-1} - 3 \frac{k^2}{D} - \frac{2}{3} ik^3 \right)^{-1}. \quad (3)$$

The second term on the right-hand side, which arises from the real part of the depolarization field, is associated with the dephasing of the field created at different points of the nanodisk and produces a shift in the position of the plasmon resonance towards larger wavelengths [43]. As we show below, the contribution of this term, which is usually overlooked, is substantial for the systems under consideration. The other term on the right-hand side is the so-called radiative correction term, which provides the radiative losses of the nanodisk that are not taken into account in the electrostatic polarizability. Therefore, this term contributes to reducing the strength of the plasmon resonance and to increasing its linewidth [43,44].

We can characterize the optical response of an individual nanodisk by calculating its extinction cross section, which, in the dipolar limit, is defined in terms of its polarizability as $\sigma_{\text{ext}} = 4\pi k \text{Im}\{\alpha\}$. Figure 1(a) displays the spectrum of σ_{ext} for a nanodisk with $D = 10 \mu\text{m}$ and $E_F = 1 \text{ eV}$. The yellow dot-dashed curve shows the results obtained using the electrostatic polarizability α_0 . As anticipated, these results depart significantly from those obtained from full solutions of Maxwell's equations solved using the finite-element method (FEM), which are plotted with the black solid curve. The FEM calculations are performed following previous works [16] and are checked for convergence with respect to all relevant discretization parameters. Examining these results, we observe that the inclusion of the radiative correction term improves the agreement of both the strength and the linewidth of the plasmon resonance, but its spectral position is still off by a significant amount. It is only when we use the fully corrected polarizability α (yellow solid curves) that we obtain a result in

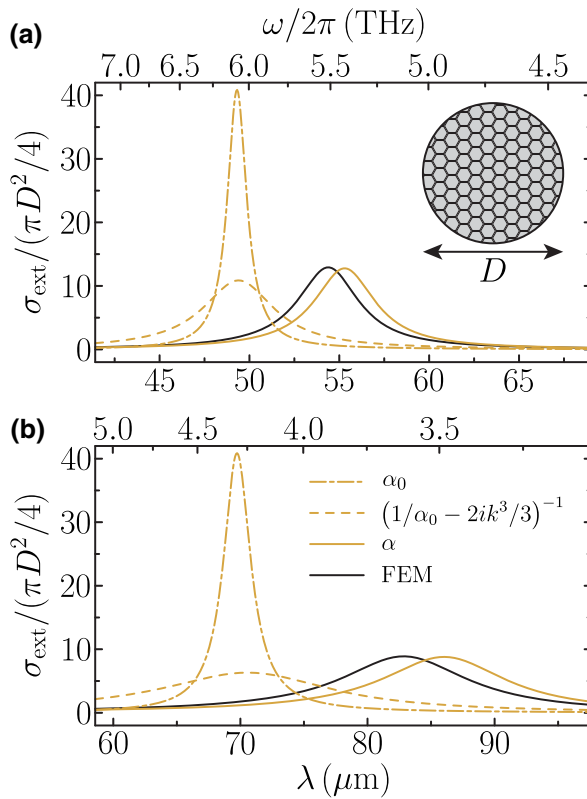


FIG. 1. Extinction cross section for an individual graphene nanodisk with diameter $D = 10 \mu\text{m}$ (a) and $D = 20 \mu\text{m}$ (b). In both cases the nanodisk is doped to a Fermi energy of $E_F = 1 \text{ eV}$. As indicated by the legend, the yellow curves display the results obtained with the PWF formalism including different levels of electrodynamic corrections as described in the main text. For comparison, the black solid curves show the results obtained using a finite-element method (FEM) approach.

excellent agreement with the FEM simulations. A similar behavior is observed for a nanodisk with $D = 20 \mu\text{m}$, shown in Fig. 1(b), although, in this case, the larger size of the nanodisk makes the electrodynamic corrections even more relevant. Importantly, with these corrections, the wavelength at which the localized plasmon resonance of the nanodisk appears in the spectrum becomes

$$\lambda_p = \sqrt{\lambda_{p,0}^2 + 12\pi^2|\eta|\xi^2D^2},$$

which confirms that the electrodynamic corrections produce a redshift of the plasmon resonance with respect to the PWF results.

Once equipped with an accurate model to describe the response of individual graphene nanodisks, we proceed to analyze the response of periodic arrays built with these nanostructures. Specifically, as sketched in Fig. 2(a), we focus on arrays with a square lattice of period a , which are located in the xy plane and surrounded by vacuum. When the array is illuminated with an electromagnetic field, the

graphene nanodisks are excited by the incident field as well as by the field scattered by the other constituents of the array. In this context, the CDM [28,32,34–36] can be used to describe the response of the array in the limit of the nanostructures being smaller than both the wavelength of light and the periodicity of the array. In our case, we choose the incident field to be a plane wave that propagates along the negative z axis and is polarized along the x axis. Due to the symmetry of the problem, we only need to consider the x component of the dipole induced in the nanodisks, which, for the nanodisk located at position \mathbf{R}_i , reads

$$p_i = \alpha E_0 + \alpha \sum_{j \neq i} G_{ij} p_j. \quad (4)$$

Here, α is the corrected polarizability of the nanodisks defined in Eq. (3), E_0 is the amplitude of the incident field, and G_{ij} is the xx component of the dipole-dipole interaction tensor, defined as $G_{ij} = [k^2 + \partial_x^2] e^{ik|\mathbf{R}_i - \mathbf{R}_j|} / |\mathbf{R}_i - \mathbf{R}_j|$. Thanks to the periodicity of the system, Eq. (4) admits the following solution in the form of a Bloch wave:

$$p = \mathcal{A}E_0.$$

Here, $\mathcal{A} = [\alpha^{-1} - \mathcal{G}]^{-1}$ is the effective polarizability of the array and $\mathcal{G} = \sum_{i \neq 0}^\infty G_{i0}$ is the lattice sum [34,36,45], which contains the information of the interaction between the elements of the array.

In order to investigate the response of the array of graphene nanodisks, we analyze the extinction efficiency of the system, which is defined in terms of the array polarizability as

$$\mathcal{E} = \frac{4\pi k}{a^2} \text{Im}\{\mathcal{A}\}. \quad (5)$$

This quantity constitutes a generalization of the extinction cross section of an individual nanodisk to an infinite array [46]. Figure 2(b) shows the extinction efficiency for different arrays of graphene nanodisks. In particular, we investigate arrays made of nanodisks with either $D = 10 \mu\text{m}$ (left column) or $D = 20 \mu\text{m}$ (right column) and a period satisfying $a/D = 2.0$ (top row), $a/D = 5.5$ (middle row), or $a/D = 7.0$ (bottom row). For each of the cases, we consider four different Fermi energies: $E_F = 0.4 \text{ eV}$ (purple curves), $E_F = 0.6 \text{ eV}$ (blue curves), $E_F = 0.8 \text{ eV}$ (red curves), and $E_F = 1.0 \text{ eV}$ (yellow curves).

Examining these results, we note that, for $a/D = 2.0$, the spectra of all of the arrays under consideration display relatively broad resonances. These resonances are located very close to the wavelength at which the individual nanodisks have their localized plasmon λ_p , which is indicated by the vertical dotted lines. In contrast, as the value of a/D is increased to 5.5 and 7.0, we observe the

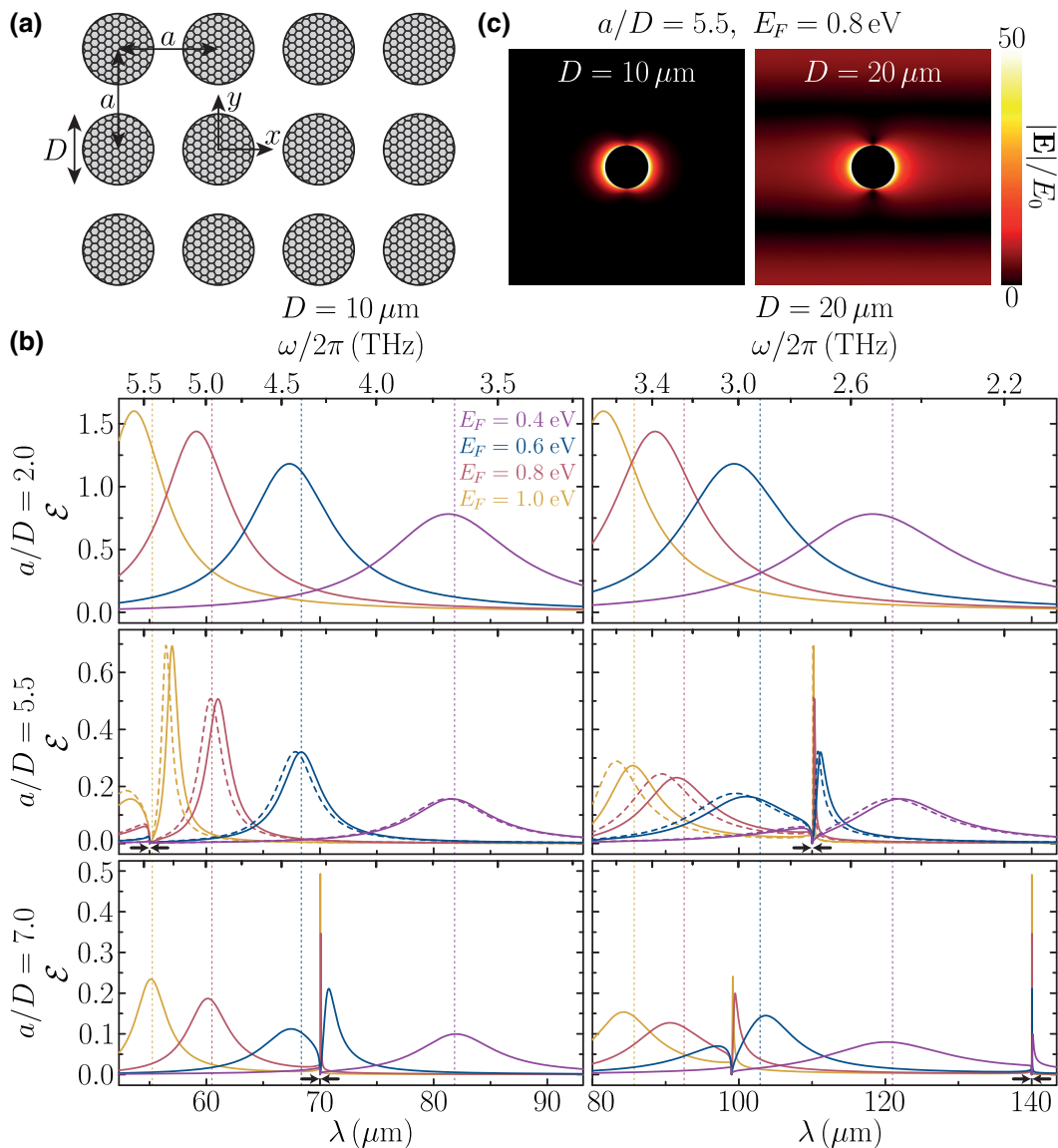


FIG. 2. (a) Schematics of a periodic array of graphene nanodisks. (b) Extinction efficiency spectra for arrays made of nanodisks with $D = 10 \mu\text{m}$ (left column) and $D = 20 \mu\text{m}$ (right column). The panels in the top, middle, and bottom rows show results for arrays with $a/D = 2.0$, $a/D = 5.5$, and $a/D = 7.0$, respectively. In all of the panels, each of the colors represents the results for a different value of E_F , as indicated by the legend located in the top left panel. For comparison, the dashed curves in the panels of the middle row show results obtained from FEM simulations. In all of the cases, the colored dotted lines indicate the value of λ_p , while the black arrows signal the position of the first Rayleigh anomaly $\lambda = a$. (c) Field amplitude $|E|$ on the unit cell, for the arrays with $a/D = 5.5$ and $E_F = 0.8 \text{ eV}$. In both cases, the results are calculated at the wavelength of maximum extinction efficiency and normalized to the amplitude of the incident field E_0 .

emergence of much narrower resonances, which appear at wavelengths slightly larger than the array period a . While the broad resonances located near λ_p completely resemble the localized plasmon of the individual nanodisks, the narrow resonances that appear at $\lambda \gtrsim a$ display the characteristics of a collective lattice resonance. The existence of these two types of resonances is connected to the relative value of λ_p and a . The reason is that, while the localized plasmon of the nanodisks is associated with the pole of

their polarizability α , lattice resonances appear at the poles of the array polarizability \mathcal{A} [34,45,47,48]. These poles are located at wavelengths larger than, but close to, the Rayleigh anomalies, where $\text{Re}\{\mathcal{G}\}$ diverges to $+\infty$. For normal incidence, the first Rayleigh anomaly appears at $\lambda = a$ (see the black arrows). Therefore, in order for the array to be able to sustain a collective lattice resonance, the localized plasmon of the nanodisks must be located at a wavelength smaller than the array period (i.e., $\lambda_p \lesssim a$).

In that way, $\text{Re}\{\alpha^{-1}\}$ can take large positive values for $\lambda \gtrsim a$, that is, in the region where $\text{Re}\{\mathcal{G}\}$ also reaches large values, thus allowing there to be the pole of \mathcal{A} [34,45,47,48]. This condition is not satisfied for any of the arrays with $a/D = 2.0$ under study, and, as anticipated, the resonance in the extinction spectra mostly corresponds to the localized plasmon of the nanodisks, with both a blueshift and an increased linewidth caused by the interaction between the elements of the array. Indeed, comparing the top left and middle left panels, we observe that both of these effects become smaller with the increase of a/D , as expected from the decrease of the interaction between the nanodisks.

The middle right and bottom left panels show a transition between the two different behaviors. While, for $E_F = 0.4$ eV, the array still displays the resonance associated with the localized plasmon of the nanodisks, for the rest of the Fermi energies under consideration, the system is able to sustain a lattice resonance. This resonance, which is located right on the red side of the first Rayleigh anomaly, has a much narrower linewidth than the plasmon of the nanodisks. The transition is completed for the array analyzed in the bottom right panel. In this case, for all values of E_F , the array displays a lattice resonance with an extremely narrow linewidth. Incidentally, in this case, we can also observe the second-order lattice resonance, which appears at wavelengths of approximately $a/\sqrt{2}$, for the two largest values of E_F .

In order to confirm the accuracy of our model, we benchmark the results displayed in the panels of the middle row against calculations obtained from FEM simulations, which are plotted with dashed curves. In all of the cases analyzed, the results of both approaches are in excellent agreement. Furthermore, we use the results of the FEM simulations to plot maps of field amplitude produced by the array for two different resonances. In particular, Fig. 2(c) shows the normalized field amplitude $|\mathbf{E}|/E_0$ over one unit cell, for the arrays with $a/D = 5.5$ and $E_F = 0.8$ eV. In both cases, the results are obtained for the wavelength at which the extinction reaches its maximum value. Examining these plots, we observe how the field amplitude for the array with $D = 10 \mu\text{m}$ only takes significant values around the nanodisk. This is the expected behavior for a resonance resembling the localized plasmon of the individual nanodisks. In contrast, for $D = 20 \mu\text{m}$, the field amplitude extends over the whole unit cell, showing fringes that change in the direction perpendicular to the polarization of the incident field. The period of these fringes is consistent with the field oscillating at $\lambda \gtrsim a$, exactly as expected from a collective lattice resonance [34]. Therefore, we conclude from the results of Fig. 2 that, as the array transitions from $a < \lambda_p$ to $a > \lambda_p$, its response evolves from a regime in which it is dominated by the localized plasmon of the individual nanodisks, with a large extinction efficiency but a broad linewidth, to another regime in which it supports a lattice resonance, resulting in a smaller

extinction efficiency but a much narrower linewidth. It is important to note that the extinction spectra of the arrays that support a lattice resonance also display the peak corresponding to the localized plasmon of the individual nanodisks, although these always produce smaller values of extinction for the systems under consideration.

One interesting aspect of the results displayed in Fig. 2(b) is that the peak value of the extinction efficiency for a fixed E_F only depends on the ratio a/D , as can be seen by comparing the curves with the same color of the panels in the same row. To understand this phenomenon and get further insight into the optical response of the arrays, in the following, we derive analytical expressions for different relevant quantities. We start by noting that, at the resonance of the array, we can approximate $\text{Re}\{\alpha^{-1} - \mathcal{G}\} \approx 0$ and, therefore, $\text{Im}\{\mathcal{A}\} \approx -1/\text{Im}\{\alpha^{-1} - \mathcal{G}\}$. Furthermore, the Weyl identity [49,50] allows us to write $\text{Im}\{\mathcal{G}\} = 2\pi k/a^2 - 2k^3/3$ for $\lambda > a$. Then, using Eqs. (3) and (5), we can write the peak value of the extinction efficiency for the resonance sustained by the array as

$$\mathcal{E}_{\text{peak}} = \frac{2}{1 + (C/E_F^2\mu)(a/D)^2}, \quad (6)$$

with $C = cv_F^2\hbar^2/(2e\xi^2)$ being a constant. Importantly, this expression predicts a peak value of the extinction efficiency that is always smaller than 2, in accordance with the theoretical limit for infinitely extended systems [51]. Furthermore, this expression confirms that, for a given value of E_F and μ , $\mathcal{E}_{\text{peak}}$ only depends on the ratio a/D .

As shown in Fig. 3, the prediction of Eq. (6) (solid curves) perfectly matches the results from the CDM calculations, which are represented with circles and crosses for arrays made of nanodisks with $D = 10 \mu\text{m}$ and $D = 20 \mu\text{m}$, respectively. This excellent agreement, which holds for all of the values of a/D and E_F under consideration, confirms the accuracy of Eq. (6) and allows us to extract some important general trends. First, the increase of a/D results in a decrease of the peak extinction efficiency, which is clearly shown by the results analyzed in Fig. 2(b). Furthermore, a larger Fermi energy and a larger mobility always contribute to increasing $\mathcal{E}_{\text{peak}}$. This is consistent with the system having a larger number of free carriers, whose density is proportional to E_F^2 , and a smaller damping coefficient γ .

The next quantity for which we want to obtain an analytical expression is the wavelength of the resonance supported by the periodic array of graphene nanodisks λ_{peak} . We analyze this quantity through the function $\Delta = \lambda_{\text{peak}}/a - 1$, which represents the normalized shift of the resonance wavelength with respect to the Rayleigh anomaly. Unfortunately, in this case, it is not possible to obtain a simple analytical expression that is valid for all of the arrays under consideration, as we did for the peak extinction efficiency. Therefore, we analyze the two

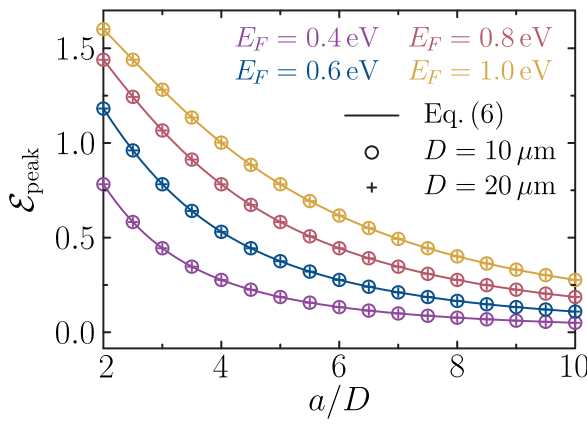


FIG. 3. Peak value of the extinction efficiency plotted as a function of a/D . The circles and crosses represent the results from the CDM calculations for arrays made of nanodisks with $D = 10\ \mu\text{m}$ and $D = 20\ \mu\text{m}$, respectively, while the solid curves correspond to the predictions of Eq. (6). Each color represents a different value of E_F , as indicated by the legend.

regimes identified in the description of Fig. 2(b) separately. For $a < \lambda_p$, as discussed above, the resonance supported by the array corresponds mostly to the localized plasmon of the individual nanodisks, with a relatively small shift caused by the interaction between the elements of the array. Therefore, we can directly write $\lambda_{\text{peak}} = \lambda_p$ and

$$\Delta_{a<\lambda_p} = \lambda_p/a - 1. \quad (7)$$

In the opposite limit, when $a > \lambda_p$, the array is able to support a lattice resonance, whose wavelength, as shown in Fig. 2(b), can strongly differ from λ_p . Therefore, to find an expression for Δ in this regime, we look for the solution of $\text{Re}\{\alpha^{-1} - \mathcal{G}\} \approx 0$. Following Refs. [28,50,52], the real part of the lattice sum of a square array can be approximated near the first Rayleigh anomaly (i.e., for $\lambda \gtrsim a$) as $\text{Re}\{\mathcal{G}\} \approx 4\pi^2\sqrt{2}/(a^3\sqrt{\lambda/a - 1}) - 118/a^3$. Using this expression, together with the definition of α given in Eq. (3), we have

$$\Delta_{a>\lambda_p} = 32\pi^4 \left[\frac{1}{|\eta|\xi^2 D^3} \frac{a^3}{\Delta_{a>\lambda_p}} \left(1 - \frac{\lambda_p^2}{a^2} \right) + 118 \right]^{-2}. \quad (8)$$

To verify the accuracy of Eqs. (7) and (8), we compare in Figs. 4(a) and 4(b) the value of $\Delta_{a<\lambda_p}$ (dashed curves) and $\Delta_{a>\lambda_p}$ (solid curves) against the results of the CDM calculations (dots). We observe that, for all of the arrays under study, the predictions of the analytical expressions are in excellent agreement with the CDM results in their corresponding regimes. As expected, the agreement deteriorates in the transition region between the two regimes. The location of this transition region, which corresponds to $\lambda_p \sim a$, has a nontrivial dependence on E_F , D , and a , but

can be visually identified as the point where $\Delta_{a<\lambda_p}$ goes to zero.

The last quantity necessary to fully characterize the resonance supported by the periodic array of graphene nanodisks is its quality factor. This quantity is defined as $Q = \lambda_{\text{peak}}/\Gamma$, with Γ being the full width at half maximum of the resonance. Noting that $\mathcal{E} \propto -\text{Im}\{\alpha^{-1} - \mathcal{G}\}/|\alpha^{-1} - \mathcal{G}|^2$ and assuming that the resonance has a Lorentzian profile, we can perform a Taylor expansion of $\alpha^{-1} - \mathcal{G}$ around the resonance wavelength and get

$$\Gamma \approx \left| \frac{2 \text{Im}\{\alpha^{-1} - \mathcal{G}\}}{(\partial/\partial\lambda) \text{Re}\{\alpha^{-1} - \mathcal{G}\}} \right|,$$

where we have assumed that $\text{Re}\{\alpha^{-1} - \mathcal{G}\} \approx 0$ and $(\Gamma/2)\partial\text{Im}\{\alpha^{-1} - \mathcal{G}\}/\partial\lambda \ll \text{Im}\{\alpha^{-1} - \mathcal{G}\}$. Importantly, all of the expressions above are to be evaluated at the wavelength of the resonance. To further simplify this expression, it is again necessary to distinguish between the two regimes discussed above. For $a < \lambda_p$, the response of the system is dominated by the localized plasmon of the individual nanodisks and, therefore, we can assume that $\partial\text{Re}\{\alpha^{-1}\}/\partial\lambda \gg \partial\text{Re}\{\mathcal{G}\}/\partial\lambda$. By doing so, we are able to write the quality factor as

$$Q_{a<\lambda_p} = \frac{\mathcal{E}_{\text{peak}}}{8\pi^2|\eta|\xi^2} \frac{a^3}{D^3} (\Delta_{a<\lambda_p} + 1). \quad (9)$$

On the other hand, for $a > \lambda_p$, we take the opposite approximation, i.e., we assume that $\partial\text{Re}\{\alpha^{-1}\}/\partial\lambda \ll \partial\text{Re}\{\mathcal{G}\}/\partial\lambda$. Therefore, in this case, we have

$$Q_{a>\lambda_p} = \frac{\mathcal{E}_{\text{peak}}}{4\sqrt{2}} \frac{1}{\Delta_{a>\lambda_p}^{3/2}}. \quad (10)$$

Interestingly, using Eq. (8), the leading term of this expression scales as $(a/D)^9$, similar to what was previously obtained for arrays of metallic nanospheres [45].

The two analytical expressions defined above provide a simple way to compute the quality factor of the resonance of the array. However, the nontrivial dependence of $\mathcal{E}_{\text{peak}}$, $\Delta_{a<\lambda_p}$, and $\Delta_{a>\lambda_p}$ on the different geometrical and material parameters of the array complicates the extraction of general trends. Therefore, to analyze the behavior of the quality factor and to verify the accuracy of the analytical expressions derived above, we plot their predictions in Figs. 4(c) and 4(d). Once again, we use dashed and solid curves to represent the results of Eqs. (9) and (10), respectively, while the dots correspond to the CDM calculations. Examining these results, we conclude that, as is the case for the normalized spectral shift, each of the analytical expressions for the quality factor is in excellent agreement with the CDM calculations within its regime of applicability. In addition, we observe that, as the system transitions from the $a < \lambda_p$ regime (dashed curves) to

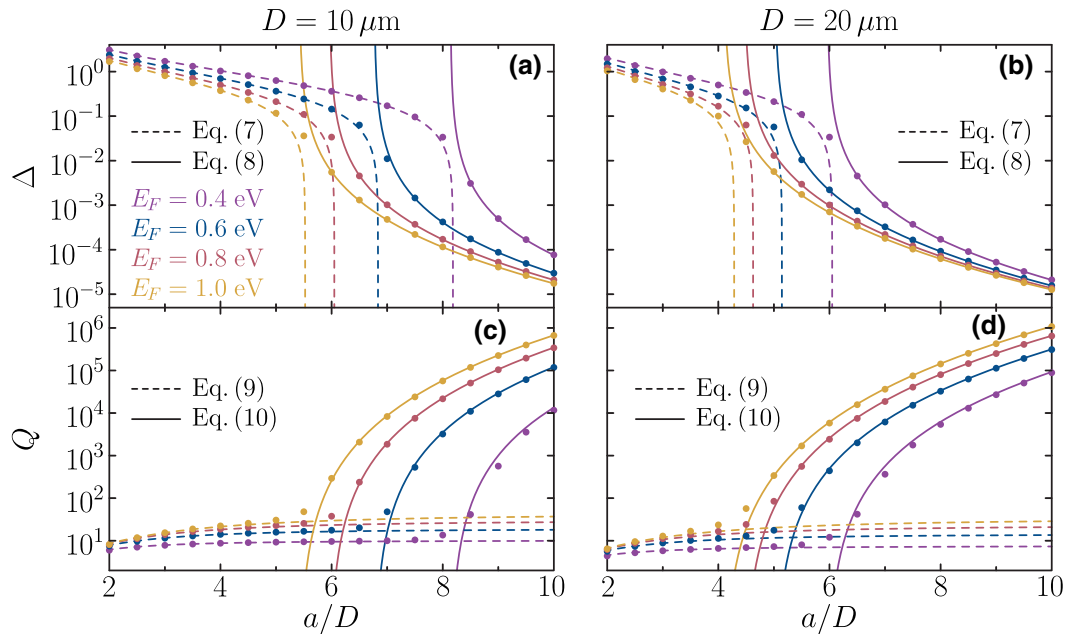


FIG. 4. Normalized spectral shift Δ (a),(b) and quality factor Q (c),(d) of the resonance of arrays made of nanodisks with either $D = 10 \mu\text{m}$ (a),(c) or $D = 20 \mu\text{m}$ (b),(d). In all of the panels, the dots indicate the results from the CDM calculations, while the dashed and solid curves represent, respectively, the predictions of Eqs. (7) and (8) in panels (a) and (b), and Eqs. (9) and (10) in panels (c) and (d). In all of the cases, the different colors correspond to different values of E_F , as indicated by the legends.

the $a > \lambda_p$ regime (solid curves), the quality factor undergoes a dramatic increase. As this happens, the value of Q becomes strongly dependent on both a/D and E_F . All of these behaviors are consistent with the resonance supported by the array changing from the localized plasmon of the individual nanodisks to a collective lattice resonance.

III. CONCLUSIONS

In summary, we have performed a comprehensive analysis of the optical response of periodic arrays of graphene nanodisks. To do so, we have introduced electrodynamic corrections to the PWF formalism, which has allowed us to describe the response of individual nanodisks beyond the electrostatic regime. Then, we have used the CDM to account for the interactions between the nanodisks in the array. With this combined approach, we have investigated the resonances supported by arrays with different geometrical and material properties, identifying two different regimes. When the period of the array is smaller than the wavelength of the localized plasmon of the nanodisks, i.e., $a < \lambda_p$, the extinction spectrum of the array displays a resonance with a large extinction efficiency but a relatively small quality factor, which resembles the localized plasmon of the individual nanodisks. In the opposite regime, i.e., $a > \lambda_p$, the array supports a lattice resonance with a much larger quality factor but a smaller extinction. Taking advantage of the simplicity of our model, we have derived

analytical expressions for the peak extinction efficiency, the wavelength, and the quality factor of the resonance supported by the array, which completely characterize the optical response of these systems in both regimes. Importantly, these expressions are valid beyond the range of parameters investigated in this work, provided the dipolar approximation is valid. Therefore, our work provides a simple and accurate theoretical tool to investigate emerging phenomena in periodic arrays of graphene nanodisks as well as to guide experimental efforts seeking to exploit the extraordinary properties of these systems.

ACKNOWLEDGMENTS

This work was sponsored by Grant No. TEM-FLU PID2019-109502GA-I00 funded by MCIN/AEI/10.13039/501100011033, as well as the U.S. National Science Foundation (Grant No. DMR-1941680). We also acknowledge support from the BBVA Foundation through a Leonardo Grant for Researchers in Physics and the CSIC (PIE 202150I030). J.R.D-R. acknowledges a predoctoral fellowship from the MCIN/AEI assigned to Grant No. PID2019-109502GA-I00. W.J.M.K-K. and D.A.R.D. acknowledge the Laboratory Directed Research and Development program of Los Alamos National Laboratory under Projects No. 20220228ER and No. 20210327ER.

APPENDIX A: ELECTRODYNAMIC CORRECTIONS TO THE PWF POLARIZABILITY

In order to incorporate the electrodynamic corrections to the PWF polarizability, we begin by writing the dipole induced in the nanodisk as

$$p = \alpha_0 (E_0 + E_d),$$

where E_d represents the electrodynamic terms of the depolarization field. To calculate this field, we assume that the induced dipole is uniformly distributed over the nanodisk and then add up the field produced by each infinitesimal surface element at the center of the nanodisk. Therefore, considering only the lowest order electrodynamic terms and exploiting the symmetry of the system, we have [43]

$$E_d = \frac{4p}{\pi D^2} \int_0^{2\pi} d\theta \int_0^{D/2} dr \left[\frac{k^2}{2} (\cos^2 \theta + 1) + i \frac{2}{3} k^3 r \right],$$

which, upon integration, results in $E_d = ((3/D)k^2 + i(2/3)k^3)p$. Then, noting that the corrected polarizability is defined as $p = \alpha E_0$, we get Eq. (3).

- [1] F. H. L. Koppens, D. E. Chang, and F. J. García de Abajo, Graphene plasmonics: A platform for strong light-matter interactions, *Nano Lett.* **11**, 3370 (2011).
- [2] A. N. Grigorenko, M. Polini, and K. S. Novoselov, Graphene plasmonics, *Nat. Photonics* **6**, 749 (2012).
- [3] F. J. García de Abajo, Graphene plasmonics: Challenges and opportunities, *ACS Photonics* **1**, 135 (2014).
- [4] L. Ju, B. Geng, J. Horng, C. Girit, M. Martin, Z. Hao, H. A. Bechtel, X. Liang, A. Zettl, Y. R. Shen, and F. Wang, Graphene plasmonics for tunable terahertz metamaterials, *Nat. Nanotechnol.* **6**, 630 (2011).
- [5] H. Yan, X. Li, B. Chandra, G. Tulevski, Y. Wu, M. Freitag, W. Zhu, P. Avouris, and F. Xia, Tunable infrared plasmonic devices using graphene/insulator stacks, *Nat. Nanotechnol.* **7**, 330 (2012).
- [6] V. W. Brar, M. S. Jang, M. Sherrott, J. J. Lopez, and H. A. Atwater, Highly confined tunable mid-infrared plasmonics in graphene nanoresonators, *Nano Lett.* **13**, 2541 (2013).
- [7] T. Guo and C. Argyropoulos, Recent advances in terahertz photonic technologies based on graphene and their applications, *Adv. Photonics Res.* **2**, 2000168 (2021).
- [8] Y. Francescato, V. Giannini, J. Yang, M. Huang, and S. A. Maier, Graphene sandwiches as a platform for broadband molecular spectroscopy, *ACS Photonics* **1**, 437 (2014).
- [9] D. Rodrigo, O. Limaj, D. Janner, D. Etezadi, F. J. García de Abajo, V. Pruneri, and H. Altug, Mid-infrared plasmonic biosensing with graphene, *Science* **349**, 165 (2015).
- [10] R. Yu, J. D. Cox, and F. J. García de Abajo, Nonlinear Plasmonic Sensing with Nanographene, *Phys. Rev. Lett.* **117**, 123904 (2016).
- [11] H. Hu, X. Yang, F. Zhai, D. Hu, R. Liu, K. Liu, Z. Sun, and Q. Dai, Far-field nanoscale infrared spectroscopy of vibrational fingerprints of molecules with graphene plasmons, *Nat. Commun.* **7**, 12334 (2016).
- [12] I. J. Luxmoore, P. Q. Liu, P. Li, J. Faist, and G. R. Nash, Graphene-metamaterial photodetectors for integrated infrared sensing, *ACS Photonics* **3**, 936 (2016).
- [13] L. Zundel and A. Manjavacas, Spatially resolved optical sensing using graphene nanodisk arrays, *ACS Photonics* **4**, 1831 (2017).
- [14] Y. Hu, A. I. López-Lorente, and B. Mizaikoff, Graphene-based surface enhanced vibrational spectroscopy: Recent developments, challenges, and applications, *ACS Photonics* **6**, 2182 (2019).
- [15] N. Rivera, I. Kaminer, B. Zhen, J. D. Joannopoulos, and M. Soljačić, Shrinking light to allow forbidden transitions on the atomic scale, *Science* **353**, 263 (2016).
- [16] S. Sanders, A. May, A. Alabastri, and A. Manjavacas, Extraordinary enhancement of quadrupolar transitions using nanostructured graphene, *ACS Photonics* **5**, 3282 (2018).
- [17] A. Ciattoni, C. Conti, and A. Marini, Multipolar terahertz absorption spectroscopy ignited by graphene plasmons, *Commun. Phys.* **2**, 111 (2019).
- [18] Y. Muniz, A. Manjavacas, C. Farina, D. A. R. Dalvit, and W. J. M. Kort-Kamp, Two-Photon Spontaneous Emission in Atomically Thin Plasmonic Nanostructures, *Phys. Rev. Lett.* **125**, 033601 (2020).
- [19] T. Guo, B. Jin, and C. Argyropoulos, Hybrid Graphene-Plasmonic Gratings to Achieve Enhanced Nonlinear Effects at Terahertz Frequencies, *Phys. Rev. Appl.* **11**, 024050 (2019).
- [20] J. D. Cox and F. J. García de Abajo, Nonlinear graphene nanoplasmonics, *Acc. Chem. Res.* **52**, 2536 (2019).
- [21] H. Cheng, S. Chen, P. Yu, J. Li, B. Xie, Z. Li, and J. Tian, Dynamically tunable broadband mid-infrared cross polarization converter based on graphene metamaterial, *Appl. Phys. Lett.* **103**, 223102 (2013).
- [22] T. Guo and C. Argyropoulos, Broadband polarizers based on graphene metasurfaces, *Opt. Lett.* **41**, 5592 (2016).
- [23] M. Liu, X. Yin, E. Ulin-Avila, B. Geng, T. Zentgraf, L. Ju, F. Wang, and X. Zhang, A graphene-based broadband optical modulator, *Nature* **474**, 64 (2011).
- [24] S. Thongrattanasiri, F. H. L. Koppens, and F. J. García de Abajo, Complete Optical Absorption in Periodically Patterned Graphene, *Phys. Rev. Lett.* **108**, 047401 (2012).
- [25] W. J. M. Kort-Kamp, A. K. Azad, and D. A. R. Dalvit, Space-Time Quantum Metasurfaces, *Phys. Rev. Lett.* **127**, 043603 (2021).
- [26] R. Yu, J. D. Cox, J. R. M. Saavedra, and F. J. García de Abajo, Analytical modeling of graphene plasmons, *ACS Photonics* **4**, 3106 (2017).
- [27] I. Silveiro, J. M. Plaza Ortega, and F. J. García de Abajo, Plasmon wave function of graphene nanoribbons, *New J. Phys.* **17**, 083013 (2015).
- [28] F. J. García de Abajo, Colloquium: Light scattering by particle and hole arrays, *Rev. Mod. Phys.* **79**, 1267 (2007).
- [29] V. G. Kravets, A. V. Kabashin, W. L. Barnes, and A. N. Grigorenko, Plasmonic surface lattice resonances: A review of properties and applications, *Chem. Rev.* **118**, 5912 (2018).
- [30] W. Wang, M. Ramezani, A. I. Väkeväinen, P. Törmä, J. Gómez Rivas, and T. W. Odom, The rich photonic world of plasmonic nanoparticle arrays, *Mater. Today* **21**, 303 (2018).

- [31] A. D. Utyushev, V. I. Zakomirnyi, and I. L. Rasskazov, Collective lattice resonances: Plasmonics and beyond, *Rev. Phys.* **6**, 100051 (2021).
- [32] L. Zhao, K. L. Kelly, and G. C. Schatz, The extinction spectra of silver nanoparticle arrays: Influence of array structure on plasmon resonance wavelength and width, *J. Phys. Chem. B* **107**, 7343 (2003).
- [33] C. L. Haynes, A. D. McFarland, L. Zhao, R. P. Van Duyne, G. C. Schatz, L. Gunnarsson, J. Prikulis, B. Kasemo, and M. Käll, Nanoparticle optics: The importance of radiative dipole coupling in two-dimensional nanoparticle arrays, *J. Phys. Chem. B* **107**, 7337 (2003).
- [34] S. Baur, S. Sanders, and A. Manjavacas, Hybridization of lattice resonances, *ACS Nano* **12**, 1618 (2018).
- [35] C. Cherqui, M. R. Bourgeois, D. Wang, and G. C. Schatz, Plasmonic surface lattice resonances: Theory and computation, *Acc. Chem. Res.* **52**, 2548 (2019).
- [36] L. Zundel, A. Cuartero-González, S. Sanders, A. I. Fernández-Domínguez, and A. Manjavacas, Green tensor analysis of lattice resonances in periodic arrays of nanoparticles, *ACS Photonics* **9**, 540 (2022).
- [37] K. I. Bolotin, K. J. Sikes, Z. Jiang, M. Klima, G. Fudenberg, J. Hone, P. Kim, and H. L. Stormer, Ultrahigh electron mobility in suspended graphene, *Sol. State Commun.* **146**, 351 (2008).
- [38] S. V. Morozov, K. S. Novoselov, M. I. Katsnelson, F. Schedin, D. C. Elias, J. A. Jaszczak, and A. K. Geim, Giant Intrinsic Carrier Mobilities in Graphene and Its Bilayer, *Phys. Rev. Lett.* **100**, 016602 (2008).
- [39] X. Wu, Y. Chuang, A. Contino, B. Sorée, S. Brems, Z. Tokei, M. Heyns, C. Huyghebaert, and I. Asselberghs, Boosting carrier mobility of synthetic few layer graphene on SiO₂ by interlayer rotation and decoupling, *Adv. Mater. Interfaces* **5**, 1800454 (2018).
- [40] Z. Fang, S. Thongrattanasiri, A. Schlather, Z. Liu, L. Ma, Y. Wang, P. M. Ajayan, P. Nordlander, N. J. Halas, and F. J. García de Abajo, Gated tunability and hybridization of localized plasmons in nanostructured graphene, *ACS Nano* **7**, 2388 (2013).
- [41] Z. Fang, Y. Wang, A. Schlather, Z. Liu, P. M. Ajayan, F. J. García de Abajo, P. Nordlander, X. Zhu, and N. J. Halas, Active tunable absorption enhancement with graphene nanodisk arrays, *Nano Lett.* **14**, 299 (2014).
- [42] C. F. Chen, C. H. Park, B. W. Boudouris, J. Horng, B. Geng, C. Girit, A. Zettl, M. F. Crommie, R. A. Segalman, S. G. Louie, and F. Wang, Controlling inelastic light scattering quantum pathways in graphene, *Nature* **471**, 617 (2011).
- [43] A. Moroz, Depolarization field of spheroidal particles, *J. Opt. Soc. Am. B* **26**, 517 (2009).
- [44] R. Yu, L. M. Liz-Marzán, and F. J. García de Abajo, Universal analytical modeling of plasmonic nanoparticles, *Chem. Soc. Rev.* **46**, 6710 (2017).
- [45] A. Cuartero-González, S. Sanders, L. Zundel, A. I. Fernández-Domínguez, and A. Manjavacas, Super- and subradiant lattice resonances in bipartite nanoparticle arrays, *ACS Nano* **14**, 11876 (2020).
- [46] L. Zundel and A. Manjavacas, Finite-size effects on periodic arrays of nanostructures, *J. Phys.: Photonics* **1**, 015004 (2019).
- [47] T. V. Teperik and A. Degiron, Design strategies to tailor the narrow plasmon-photonic resonances in arrays of metallic nanoparticles, *Phys. Rev. B* **86**, 245425 (2012).
- [48] L. Zundel, J. R. Deop-Ruano, R. Martínez-Herrero, and A. Manjavacas, Lattice resonances excited by finite-width light beams, *ACS Omega* **7**, 31431 (2022).
- [49] L. Novotny and B. Hecht, *Principles of Nano-Optics* (Cambridge University Press, New York, 2006).
- [50] A. Manjavacas, L. Zundel, and S. Sanders, Analysis of the limits of the near-field produced by nanoparticle arrays, *ACS Nano* **13**, 10682 (2019).
- [51] V. A. Markel, Extinction, scattering and absorption of electromagnetic waves in the coupled-dipole approximation, *J. Quantum Spectrosc. Radiat. Transf.* **236**, 106611 (2019).
- [52] F. J. García de Abajo, R. Gómez-Medina, and J. J. Sáenz, Full transmission through perfect-conductor sub-wavelength hole arrays, *Phys. Rev. E* **72**, 016608 (2005).